Theoretical extension of the gold pressure calibration standard beyond 3 Mbars

J. C. Boettger
Applied Physics Division, Los Alamos National Laboratory, Los Alamos, New Mexico 87545
(Received 20 November 2002; revised manuscript received 12 March 2003; published 16 May 2003)

The static-lattice equation of state and structural phase stability of gold have been calculated to 10 Mbar, using two distinct density functional models; the local density approximation (LDA) and the generalized gradient approximation (GGA). The fcc structure is predicted to be the most stable phase at zero pressure, transforming to the hcp structure at 3.5 Mbar (LDA) or 4.1 Mbar (GGA), which then remains stable to 10 Mbar. These transition pressures are roughly 50% larger than previous predictions. Once thermal effects are accounted for, the LDA model produces a room temperature isotherm that is in rather good agreement with existing data and that smoothly merges with the existing gold pressure calibration standard near 2 Mbar. The LDA room temperature isotherm should provide a reliable extension of the gold pressure calibration standard up to the fcc-hcp transition pressure, well above 3 Mbar.

DOI: 10.1103/PhysRevB.67.174107 PACS number(s): 64.30.+t, 64.70.Kb

I. BACKGROUND

Gold (Au) has been employed as a primary equation of state (EOS) standard, for at least two decades,[1] due to its chemical inertness, large isothermal compressibility, and the large pressure and temperature stability ranges of its ambient fcc phase. For this reason, the room temperature isotherm of Au has been determined for pressures up to 2.16 Mbar,[2] through a combination of diamond anvil cell (DAC) data up to 700 kbar (Refs. 2 and 3) and reduced shock data at the higher pressures.[1,2] Although the existing Au pressure calibration standard[2] is adequate for most static experiments carried out today, improved DAC techniques have extended the experimentally accessible pressure range to at least 3 Mbar,[4] with even higher pressures on the horizon. As a result, there is a growing need for reliable EOS standards in the 2–10 Mbar range. The most straightforward way to achieve this goal would be to extend the range of the existing EOS standards to higher pressures using some mixture of high-pressure shock data and first-principles theory,[5] including density functional theory[6] (DFT) electronic structure calculations.

Although DFT electronic structure calculations have not been demonstrated to reliably predict pressure-volume curves to the accuracy required for an EOS standard, such calculations do provide valuable qualitative guidance. In particular, the two most common models, the local density approximation (LDA) (Ref. 7) and the generalized gradient approximation (GGA),[8] generally have been found to produce pressures that provide approximate lower (LDA) and upper (GGA) bounds to the observed pressure for a given volume. It is also known that those two bounds will converge (presumably to the correct value) in the ultrahigh pressure limit. Furthermore, DFT calculations have been used successfully to predict structural phase sequences in crystalline materials. Thus, DFT electronic structure calculations should be expected to play an important role in extending the Au pressure calibration standard to multi-Mbar pressures.

A number of DFT electronic structure calculations already have been carried out on the static-lattice, zero-pressure properties of Au.[9–16] Only two of those calculations, however, have explored the multi-Mbar regime.[9,15] In the earlier of those investigations, Godwal and Jeanloz[9] determined the EOS of fcc Au to 2 Mbar using the linear muffin-tin-orbital (LMTO) method, within the atomic sphere approximation (ASA) and the LDA model. Once thermal effects were accounted for, the LDA-derived room temperature isotherm was found to be in reasonable agreement with the existing Au standard. In the later study, Ahuja *et al.*[15] used the presumably more precise full-potential LMTO (FP-LMTO) method, within both the LDA and GGA models, to calculate the energy difference between the ambient fcc phase of Au and a hypothetical hcp phase, for volumes ranging from ambient to two-fold compressed. Those calculations predicted that Au would transform into the hcp structure at a pressure of either 2.41 Mbar (LDA) or 2.00 Mbar (GGA), calling into question the usefullness of Au as a pressure standard above 2 Mbar. The transition point found using the LDA was, however, inconsistent with the isotherm obtained by Godwal and Jeanloz[9] using the same model; see discussion below. In addition, Ahuja *et al.*[15] did not consider the possibility of bcc phase stability, despite the fact that the fcc and bcc phases are known to be nearly degenerate at zero pressure, with two LDA calculations predicting bcc stability[17,18] and one predicting fcc stability.[19] This omission is surprising, since one of the predictions of bcc stability[18] was obtained using the same FP-LMTO code as was used by Ahuja *et al.*[15]

In this investigation, the static-lattice EOS and structural phase stability of fcc, bcc, and ideal hcp Au have been calculated to about 10 Mbar, using a relativistic variant[20–22] of the all-electron linear combinations of Gaussian-type-orbitals–fitting-function (LCGTO-FF) method,[23,24] as implemented in the program package GTOFF.[25] The LDA and GGA models were both used here to provide approximate lower and upper bounds to the true pressures, and to allow an estimate of any model sensitivity in the predicted phase sequence. All of the calculations for the cubic structures were carried out with and without spin-orbit coupling (SOC) effects included. Room temperature thermal corrections to the pressures were calculated for the observed fcc phase. Since the results presented here are intended for use in extending

the Au pressure calibration standard, extensive tabular results are provided.

II. LCGTO-FF ELECTRONIC STRUCTURE CALCULATIONS

The LCGTO-FF technique is distinguished from other variants of the LCGTO methodology through its use of auxiliary GTO basis sets to expand the charge density and exchange-correlation (XC) integral kernels. The charge fitting function coefficients are determined variationally by minimizing the error in the Coulomb energy, while the XC coefficients are obtained via a constrained least squares fit. Scalar relativity was first implemented[20] in GTOFF using a nuclear-only Douglas-Kroll-Hess (nDKH) transformation,[26,27] that neglected all terms involving cross products of the momentum operator.[28] That implementation of relativity was later extended to include all scalar relativistic cross-product terms and spin-orbit coupling terms produced by the nDKH transformation.[21] Finally, electron-electron spin-orbit coupling effects were accounted for within the screened nuclear spin-orbit (SNSO) approximation.[22] The LCGTO-FF method is especially well adapted for high-pressure EOS work because, unlike most extant DFT electronic structure methods, it does not require the electrons to be partitioned between core and band states that are treated differently. Instead, GTOFF treats all electron states as fully hybridizing band states. Furthermore, the spin-orbit coupling terms calculated with GTOFF are not afflicted with the muffin-tin-sphere sensitivity observed in some other full-potential methods.[22]

The precision of any LCGTO-FF calculation is largely determined by the selection of the three GTO basis sets. The orbital basis set used here was derived from Gropen's[29] $19s14p10d5f$ atomic basis set. First, the more diffuse portion of the atomic basis set was modified and enriched, to provide a better representation of the crystalline environment, yielding a $20s16p12d8f$ primitive GTO basis. That basis set was then reduced to a $15s12p9d5f$ basis set by contracting the most local GTO's of each l type into a single basis function, using contraction coefficients obtained from scalar-relativistic atomic calculations with the same DFT models as the crystal calculations; i.e., slightly different coefficients were used for the LDA and GGA calculations. The electronic charge density was fitted, for volumes near ambient, with a $21s$ GTO basis set whose exponents ranged from 0.1 to 2 500 000. An $18s$ XC basis set was derived from the charge basis set by removing the three most local GTO's. The same basis sets were used, for a given model, for all of the calculations corresponding to fcc lattice constants greater than 7.3 Bohr. For smaller volumes, the more diffuse GTO's in the three basis sets were gradually compressed, as needed, to avoid near linear dependencies. It is quite difficult to quantify the uncertainty in the energies due to the use of incomplete basis sets. It is, however, reasonable to assume that the relative errors between the various structures will be quite small (on the order of 0.1 mRy) and smoothly varying, since the absolute errors will largely cancel for a given atomic volume. All of the basis sets used here can be obtained from the author.

All necessary Brillouin zone (BZ) integrations were carried out on uniform BZ meshes using a Gaussian broadened histogram technique, with a Gaussian broadening factor of 10 mRy. Test calculations revealed that the fcc-bcc structural energy difference, at ambient volume, was sensitive to the density of the BZ mesh, with higher mesh densities favoring the fcc structure. This BZ mesh sensitivity may account, in part, for the disagreement between the earlier structural stability calculations; see discussion above. For the fcc and bcc structures, a $20\times20\times20$ BZ mesh with 256 inequivalent k points was used to ensure that the ambient fcc-bcc structural energy difference was converged to within 0.1 mRy. This uncertainty in the structural energy difference should increase steadily as the unit cell volume decreases, due to the corresponding expansion of the BZ, with any resulting error varying smoothly with volume. A comparable $20\times20\times10$ BZ mesh with 264 inequivalent k points was used for the hcp structure and should produce a similar uncertainty. The SCF cycle for each calculation was iterated until the total energy was stable to within 20 μRy, which should be the primary source of random error in these calculations.

III. RESULTS

LDA and GGA total energies were first calculated for fcc Au, with and without spin-orbit coupling, for lattice constants ranging from 8.0 to 7.0 Bohr in steps of 0.1 Bohr and from 7.0 to 6.0 Bohr in steps of 0.2 Bohr. Three additional GGA calculations were then carried out at fcc lattice constants of 8.1, 8.2, and 8.3 Bohr, to ensure that the GGA energy minimum was bracketted. Cohesive energies were obtained by removing spin-polarized atomic energies, calcu-

TABLE I. LDA binding energies (E_b; Ry) obtained here, with and without spin-orbit coupling (SOC) effects included, are listed as functions of the fcc lattice constant (a; Bohr) for fcc, bcc, and hcp Au.

a	fcc	bcc	hcp	fcc+SO	bcc+SO
8.00	−0.32327	−0.32232	−0.32230	−0.33327	−0.33226
7.90	−0.32863	−0.32765	−0.32749	−0.33893	−0.33784
7.80	−0.33263	−0.33149	−0.33129	−0.34323	−0.34195
7.70	−0.33487	−0.33363	−0.33342	−0.34578	−0.34446
7.60	−0.33513	−0.33381	−0.33359	−0.34641	−0.34491
7.50	−0.33305	−0.33161	−0.33154	−0.34478	−0.34318
7.40	−0.32822	−0.32663	−0.32681	−0.34048	−0.33882
7.30	−0.32014	−0.31865	−0.31894	−0.33293	−0.33131
7.20	−0.30986	−0.30830	−0.30871	−0.32303	−0.32137
7.10	−0.29322	−0.29166	−0.29212	−0.30673	−0.30521
7.00	−0.27059	−0.26895	−0.26956	−0.28452	−0.28279
6.80	−0.20298	−0.20135	−0.20209	−0.21780	−0.21606
6.60	−0.09970	−0.09866	−0.09926	−0.11519	−0.11399
6.40	0.04700	0.04768	0.04683	0.03000	0.03093
6.20	0.25606	0.25566	0.25442	0.23665	0.23660
6.00	0.55816	0.55599	0.55534	0.53572	0.53365

TABLE II. GGA binding energies (E_b; Ry) obtained here, with and without spin-orbit coupling (SOC) effects included, are listed as functions of the fcc lattice constant (a; Bohr) for fcc, bcc, and hcp Au.

a	fcc	bcc	hcp	fcc+SO	bcc+SO
8.30	−0.23020	−0.22996	−0.22951	−0.23846	−0.23808
8.20	−0.23496	−0.23455	−0.23413	−0.24353	−0.24292
8.10	−0.23887	−0.23831	−0.23790	−0.24779	−0.24708
8.00	−0.24173	−0.24110	−0.24056	−0.25097	−0.25026
7.90	−0.24331	−0.24267	−0.24196	−0.25283	−0.25216
7.80	−0.24337	−0.24265	−0.24178	−0.25318	−0.25240
7.70	−0.24147	−0.24068	−0.23977	−0.25173	−0.25079
7.60	−0.23747	−0.23661	−0.23563	−0.24809	−0.24703
7.50	−0.23086	−0.22995	−0.22904	−0.24192	−0.24082
7.40	−0.22132	−0.22055	−0.21961	−0.23292	−0.23197
7.30	−0.20832	−0.20755	−0.20678	−0.22040	−0.21948
7.20	−0.19303	−0.19226	−0.19151	−0.20553	−0.20459
7.10	−0.17118	−0.17044	−0.16974	−0.18407	−0.18324
7.00	−0.14297	−0.14224	−0.14157	−0.15628	−0.15542
6.80	−0.06341	−0.06259	−0.06241	−0.07762	−0.07678
6.60	0.05293	0.05363	0.05351	0.03767	0.03844
6.40	0.21366	0.21432	0.21350	0.19724	0.19786
6.20	0.44324	0.44378	0.44201	0.42477	0.42489
6.00	0.77373	0.77208	0.77091	0.75145	0.74929

lated with GTOFF in the expanded lattice limit, using the same models as were used for the crystal calculations.[30] Similar calculations were then carried out for the bcc and ideal hcp crystal structures using atomic volumes that were identical to those used for the fcc structure. (Spin-orbit coupling was not, however, considered for the hcp phase.) All of the LDA and GGA cohesive energies so determined are listed in Tables I and II, respectively. (The number of figures given in the tables are consistent with the random error in the energies 20 μRy, not the overall precision; see the preceding discussion.) Note that, for all models, the most stable phase is the fcc structure at the larger lattice constants, transforming to the hcp structure at the smaller lattice constants, with no region of bcc stability.

A. Zero-pressure properties

For each model and crystal structure, the zero-pressure volume (V_0), cohesive energy (E_c), bulk modulus (B), and pressure derivative of the bulk modulus (B') were determined by fitting the cohesive energies of the eight (LDA) or eleven (GGA) largest volumes with the stabilized jellium equation of state (SJEOS) of Alchagirov *et al.*[31]

$$\epsilon(x) = \frac{a}{x^3} + \frac{b}{x^2} + \frac{c}{x} + d, \tag{1}$$

where

$$x = \left(\frac{V}{V_0}\right)^{1/3}. \tag{2}$$

TABLE III. Theoretical static-lattice, zero-pressure volumes (V_0; a.u.), cohesive energies (E_c; Ry), bulk moduli (B; Mbar), and pressure derivatives of the bulk moduli (B') obtained here for fcc Au using the LDA and GGA models, both with and without spin-orbit coupling (SOC) included, are compared to previous full-potential calculations and experiment.

Method	Model	V_0	E_c	B	B'
FLAPW[a]	LDA	112.4		1.98	
FP-LMTO[b]	LDA	113.2		1.93	
FLAPW[c]	LDA	112.9		2.05	
LCAO[d]	LDA+SOC	112.99		1.82	
FP-LMTO[e]	LDA	113.10		1.93	4.8
FP-LMTO[f]	LDA	113.41		1.76	6.1
LCGTO-FF[g]	LDA	111.36	0.3353	1.90	5.1
LCGTO-FF[g]	LDA+SOC	110.60	0.3465	1.92	5.1
FLAPW[a]	GGA	121.4		1.42	
FP-LMTO	GGA	118.23		2.19	3.7
LCAO[h]	GGA	123.7	0.209	1.32	
LCAO[h]	GGA+SOC	122.3	0.220	1.30	
LCGTO-FF[g]	GGA	120.87	0.2435	1.42	5.5
LCGTO-FF[g]	GGA+SOC	119.95	0.2533	1.45	5.4
Experiment[a]	0 K	112.8			
Experiment[i]	298 K	114.45	0.279	1.67	5.5

[a]Reference 10.
[b]Reference 11.
[c]Reference 12.
[d]Reference 13.
[e]Reference 15.
[f]Reference 16.
[g]Present results.
[h]Reference 14.
[i]Reference 2, except E_c which is taken from Ref. 32.

In Eq. (1), the four terms on the right-hand side (RHS) roughly correspond to the the energy contributions of the repulsive (non-Coulombic) part of an electron-ion pseudopotential, the kinetic energy, the combined Madelung and exchange energies, and the correlation energy. The results of these fits are compared with previous calculations and experiment in Tables III (fcc) and IV (bcc and ideal hcp).

Examination of Table III reveals good consistency between the various results obtained using a given model, with no notable sensitivity to spin-orbit coupling. The LDA and GGA volumes found here with the LCGTO-FF method are 2% contracted and 6% expanded, respectively, relative to the empirical static-lattice volume.[10] These results are consistent with the general expectation that the LDA and GGA models will produce volumes that bound the experimental value. The LDA and GGA bulk moduli found here also bracket the measured room temperature value, with the LDA value being 15% larger and the GGA value being 13% smaller. Although the GGA values for B and B' appear to be in better agreement with experiment than the LDA values, much of the error in the LDA values is attributable to the difference between the theoretical static-lattice volume and the observed room temperature volume. In fact, the fitted LDA+SOC values for B and B' at the experimental volume are 1.60 Mbar

TABLE IV. Theoretical static-lattice, zero-pressure volumes (V_0; a.u.), cohesive energies (E_c; Ry), bulk moduli (B; Mbar), and pressure derivatives of the bulk moduli (B') obtained here for bcc and ideal hcp Au using the LDA and GGA models, both with and without spin-orbit coupling (SOC) included, are listed. Also shown are FP-LMTO results for hcp Au from Ref. 15.

Method	Model	V_0	E_c	B	B'
bccStructure					
LCGTO-FF	LDA	111.62	0.3340	1.87	4.9
LCGTO-FF	LDA+SOC	110.84	0.3450	1.98	4.9
LCGTO-FF	GGA	121.05	0.2428	1.39	5.6
LCGTO-FF	GGA+SOC	120.18	0.2524	1.43	5.3
hcpStructure					
FP-LMTO	LDA	111.35		1.91	4.7
LCGTO-FF	LDA	111.49	0.3338	1.83	5.0
FP-LMTO	GGA	116.88		2.16	3.7
LCGTO-FF	GGA	121.38	0.2421	1.37	5.3

and 5.4, respectively, in excellent agreement with the measured values; 1.67 Mbar and 5.5.

Comparison of the LCGTO-FF results found here for the bcc and ideal hcp structures of Au (Table IV) with the fcc structure results in Table III reveals only a minimal structure-induced variation of the zero-pressure properties. To be specific, the atomic volumes, bulk moduli and pressure derivatives of the bulk moduli for the three structures vary by roughly 0.5, 2, and 8 %, respectively. In contrast, Ahuja *et al.*[15] found a volume shift of more than 1% between the fcc and hcp structures. For a given model, the cohesive energies predicted for the three structures agree to within roughly 1.5 mRy, with the fcc structure being somewhat more stable than the bcc structure at zero pressure, in good agreement with experiment. For the observed fcc structure, the LDA model produces a substantial overbinding relative to experiment,[32] while the GGA model predicts a smaller underbinding.

All of these zero-pressure results are in good accord with the standard expectations for state-of-the-art DFT electronic structure calculations. The most notable finding, in the context of this work, is that the LDA model yields rather good agreement with the existing zero-pressure data and is clearly preferable to the GGA model for determining the low pressure EOS of this particular material. This result also serves as a reminder that there are a number of systems for which the LDA model works better than the presumptively more advanced GGA model.[10,33]

B. High-pressure properties

To allow a more direct comparison of the present LDA and GGA electronic structure results with high pressure data, room temperature isotherms were constructed for fcc Au, as follows. First, all of the fcc cohesive energies listed in Tables I and II for a given DFT model, with spin-orbit coupling included, were fitted to the SJEOS. Phonon contributions were then estimated, at room temperature, using a simple

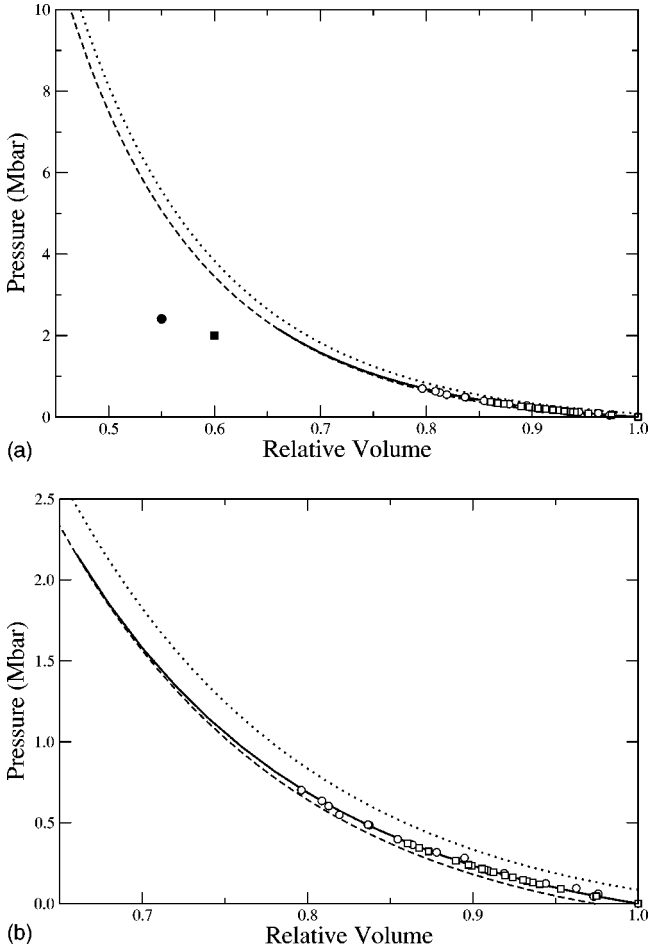

FIG. 1. Room temperature isotherms for fcc Au obtained here using the LDA (dashed line) and GGA (dotted line) are compared with diamond anvil cell data from Refs. 2 (open circles) and 3 (open squares), and the gold standard of Ref. 2 (solid line); (a) for pressures up to 10 Mbar and (b) for pressures up to 2.5 Mbar. Also shown are the fcc-hcp phase transition points obtained by Ref. 15 using the LDA (filled circle) and GGA (filled square) models. Volumes are given relative to the experimental room temperature volume, 114.445 a.u.

Debye model, with the ambient value of the Debye temperature (θ_D) set to its observed value 165 K.[34] The volume dependence of θ_D was specified via a Grüneisen function (γ) of the form

$$\gamma(x) = \gamma_0 x + \frac{2}{3}(1-x)^2, \tag{3}$$

where $x = V/V_0$ is the relative volume, V_0 is the experimentally observed room temperature volume (114.445 a.u.), and γ_0 is the ambient value of γ (3.05).[34] Contributions of thermal electronic excitations were not calculated here, since they should be negligible at room temperature.

The LDA and GGA room temperature isotherms determined here for fcc Au, as described above, are compared to DAC data[2,3] and the Au pressure standard of Heinz and Jeanloz[2] in Fig. 1. Inspection of the figure reveals that the LDA isotherm is, once again, in substantially better agree-

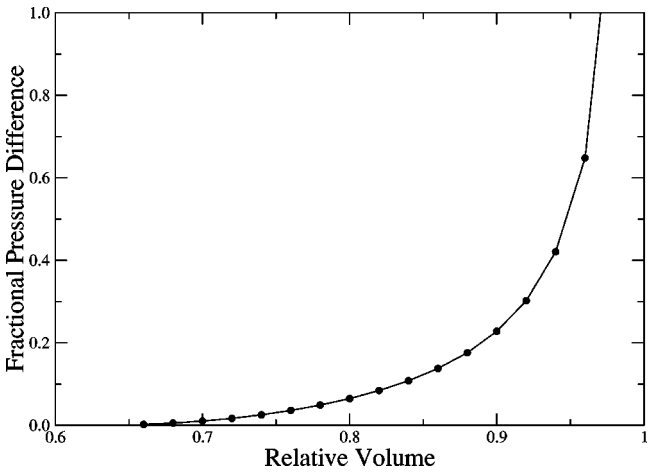

FIG. 2. The fractional difference between the LDA room temperature pressure of fcc Au and the pressure standard of Ref. 2 is shown as a function of relative volume.

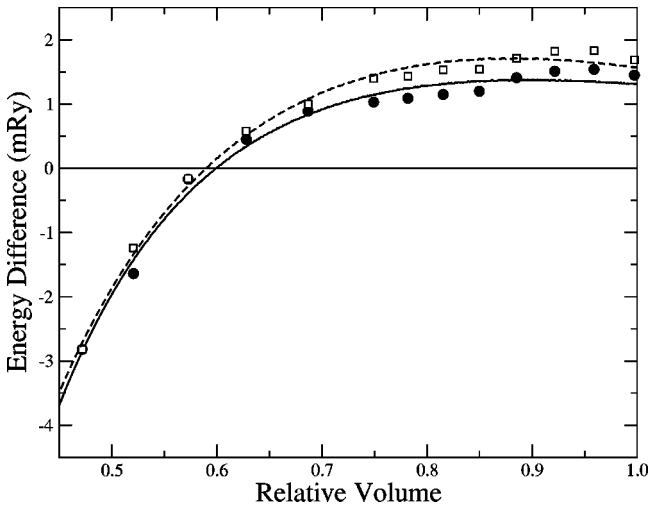

FIG. 3. Calculated and fitted hcp-fcc structural energy differences for Au obtained here with the LDA (circles; solid line) and GGA (squares; dashed line) models are shown as functions of relative volume.

ment with the data than the GGA isotherm. In particular, the LDA pressures appear to merge smoothly with the Au standard near 2 Mbar, as is further illustrated in Fig. 2, which shows the fractional difference between the LDA pressure (P_{LDA}) and the pressure of the Au standard (P_s),

$$f = \frac{P_s - P_{\mathrm{LDA}}}{P_s}, \tag{4}$$

as a function of relative volume. These results are consistent with the expectation that LDA pressures act as an approximate lower bound to experiment and suggest that the LDA isotherm may provide a reliable extension of the existing Au standard beyond 2 Mbar. Naturally, such an extension will only be reasonable up to the fcc-hcp transition pressure.

The hcp-fcc structural energy differences determined here for Au, using the LDA and GGA models, are shown as functions of relative volume in Fig. 3. Although the energy differences are somewhat noisy, it is obvious that both models yield a transition volume that is roughly 60% of the measured ambient volume for fcc Au. To obtain a more precise estimate for the fcc-hcp transition volume, the LDA and GGA cohesive energies for both phases were fitted with the SJEOS. A smooth fit to the calculated structural energy differences was then obtained for each model by taking the difference between the binding curves for the two crystal structures. The fitted energy difference curves are compared with the calculated differences in Fig. 3. Examination of the figure suggests that the energy differences have a smoothly varying, model independent, uncertainty that is on the order of 2–3 mRy, in reasonable agreement with the error analysis given above. The fitted curves were used to obtain LDA and GGA predictions for the pressure and volume of the fcc-hcp transition in Au on the static-lattice 0 K isotherm.

The transition volumes and pressures obtained here are listed in Table V along with the corresponding values found by Ahuja *et al.*[15] Although the transition volumes found in the two investigations are in reasonable agreement, the pressures differ greatly. In particular, the relative volumes calculated using the GGA differ by only 0.01, yet the transition pressures differ by a factor of 2. Comparison of the GGA and LDA transition points found by Ahuja *et al.*,[15] with the various isotherms in Fig. 1 strongly suggests that the pressure calculation by Ahuja *et al.*,[15] is in error. The present calculations indicate that the fcc phase of Au will remain stable relative to the hcp and bcc phases for pressures well in excess of 3 Mbar.

There remains the possibility that Au transforms into a structure that is more complicated than any of those considered here, as has been demonstrated for the light[35] and heavy[36] alkali metals. In those cases, the structural phase transitions are triggered by electronic transitions; $s \rightarrow p$ for the light alkali metals[37] and $s \rightarrow d$ for the heavy alkali metals.[38] The equivalent mechanism for Au would be a $6s \rightarrow 6p/5f$ transition. To explore this possibility, the scalar-relativistic LDA electronic band structures obtained here for fcc Au at lattice constants of 7.70 Bohr (near $P = 0$ Mbar) and 6.00 Bohr (near $P = 10$ Mbar) are shown in Figs. 4 and 5, respectively. Comparison of the occupied bands in the figures suggests that nearly all of the qualitative features are insensitive to pressure, other than an overall broadening. (The same is not true of the conduction bands, which are

TABLE V. Predicted relative volumes (V/V_0) and pressures (P; Mbar) of the fcc-hcp transition in Au obtained here with the LCGTO-FF method, using the LDA and GGA models, are compared with equivalent FP-LMTO results from Ref. 15. V_0 is the experimental room temperature volume.

Method	Model	V/V_0	P
LCGTO-FF	LDA	0.599	3.47
FP-LMTO	LDA	0.55	2.41
LCGTO-FF	GGA	0.590	4.14
FP-LMTO	GGA	0.60	2.00

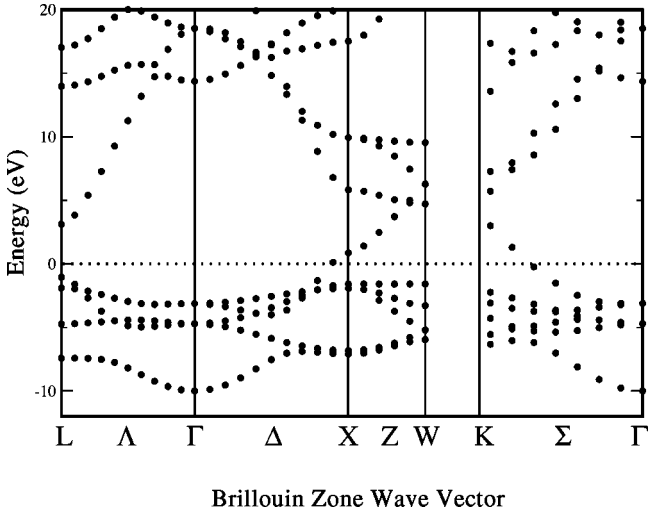

FIG. 4. Scalar-relativistic LDA electronic band structure for fcc Au at a lattice constant of 7.70 Bohr. The energies are given relative to the Fermi level; dotted line.

highly distorted.) The most notable change in the occupied band structure is the movement of one energy at the *X* point from above the Fermi level to below. These results are in good agreement with Godwal and Jeanloz,[9] who found no evidence for an electronic transition in Au, up to 2 Mbar, and Ahuja *et al.*[15] who concluded that the fcc-hcp transition is triggered by relatively small features in the densities of states for the two structures. Even if an electronic transition did occur in Au, it would affect less than 10% of the eleven valence electrons versus 100% of the valence electrons in an alkali metal, thus providing a substantially weaker mechanism for phase transitions in Au. Nevertheless, further work on the structural stability of Au at high pressures is clearly warranted.

Based on the above analysis, the theoretical room temperature isotherm found here using the LDA should provide a reliable extension of the existing Au pressure calibration standard beyond 3 Mbar. To provide easy access to this extension, the LDA isotherm is tabulated in Table VI on a rather dense mesh of relative volumes, along with the Au standard of Heinz and Jeanloz.[2] Given the uncertainties inherent in predicted structural transition pressures and the possibility of metastability beyond the equilibrium phase boundary, the new isotherm is tabulated up to roughly 5 Mbar. During experiments, the standard of Heinz and Jeanloz should be used for relative volumes between 1.0 and 0.66, while the LDA isotherm should be used for all relative volumes less than 0.66, provided the fcc structure remains stable.

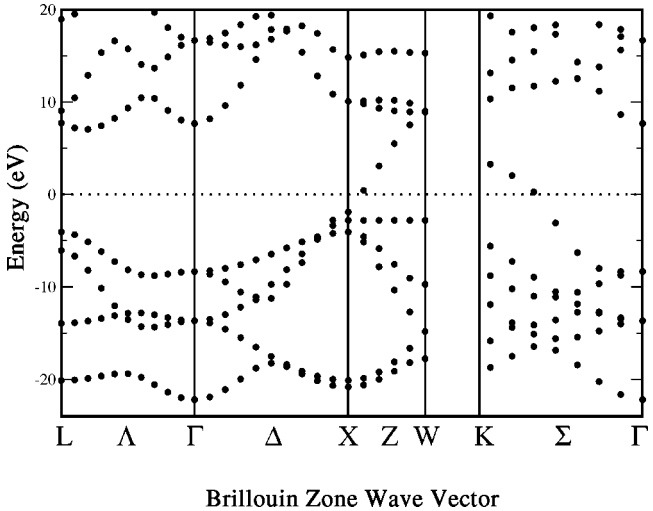

FIG. 5. Scalar-relativistic LDA electronic band structure for fcc Au at a lattice constant of 6.00 Bohr. The energies are given relative to the Fermi level; dotted line.

TABLE VI. The theoretical room temperature isotherm (Mbar) obtained here for fcc Au, using the LDA, is tabulated as a function of relative volume, up to 5 Mbar. The existing gold pressure calibration standard of Heinz and Jeanloz (HJ) (Ref. 2) is also listed.

V/V_0	LDA	HJ	V/V_0	LDA	HJ
1.00	−0.0435	0.0000	0.70	1.5630	1.5790
0.98	−0.0111	0.0356	0.68	1.8386	1.8484
0.96	0.0268	0.0761	0.66	2.1567	2.1610
0.94	0.0708	0.1222	0.65	2.3338	
0.92	0.1219	0.1746	0.64	2.5244	
0.90	0.1810	0.2344	0.63	2.7294	
0.88	0.2492	0.3024	0.62	2.9502	
0.86	0.3277	0.3800	0.61	3.1881	
0.84	0.4180	0.4685	0.60	3.4446	
0.82	0.5218	0.5697	0.59	3.7213	
0.80	0.6410	0.6854	0.58	4.0200	
0.78	0.7779	0.8179	0.57	4.3427	
0.76	0.9352	0.9700	0.56	4.6916	
0.74	1.1160	1.1449	0.55	5.0691	
0.72	1.3238	1.3464			

IV. CONCLUSIONS

The static-lattice EOS and structural phase stability of Au have been calculated to 10 Mbar, with and without spin-orbit coupling effects included, using the LDA and the GGA. It is shown that spin-orbit coupling effects are negligible, while density gradient corrections are significant. The calculated zero-pressure properties of Au agree well with results from previous electronic structure calculations using the same models. The fcc structure is predicted to be more stable than the hcp and bcc structures at zero pressure, in good agreement with experiment. The hcp structure becomes the most stable structure at a pressure of 3.5 Mbar (LDA) or 4.1 Mbar (GGA) and remains stable to 10 Mbar. These transition pressures are roughly 50% larger than previous predictions,[15] due to some error in the earlier pressure calculations.

Once thermal effects are accounted for, the LDA model produces a room temperature isotherm that is in reasonably good agreement with existing data and that smoothly merges with the existing Au pressure calibration standard[2] near 2 Mbar. The room temperature isotherm found here with the LDA model should, therefore, provide a reliable extension of

the existing gold standard up to the fcc-hcp transition pressure, well above 3 Mbar. Additional DAC experiments will be needed to test the reliablity of the new Au standard against other EOS standards, such as tungsten and copper, and to determine more accurately where the fcc-hcp transition occurs along the room temperature isotherm.

ACKNOWLEDGMENTS

I am grateful to J. D. Johnson for helpful suggestions during this investigation. This work was supported by the U. S. Department of Energy under Contract No. W-7405-ENG-36.

[1] J. C. Jamieson, J. N. Fritz, and M. H. Manghnani, *High-Pressure Research in Geophysics*, edited by S. Akimoto and M. H. Manghnani (Center for Academic Publishing, Tokyo, 1982), p. 27.
[2] D. L. Heinz and R. Jeanloz, J. Appl. Phys. **55**, 885 (1984).
[3] T. S. Duffy, G. Shen, D. L. Heinz, J. Shu, Y. Ma, H. K. Mao, R. J. Hemley, and A. K. Singh, Phys. Rev. B **60**, 15063 (1999); J. Appl. Phys. **86**, 6729 (1999).
[4] See, for example, L. S. Dubrovinsky, S. K. Saxena, F. Tutti, S. Rekhi, and T. LeBehan, Phys. Rev. Lett. **84**, 1720 (2000).
[5] See, for example, the extension of the copper standard to 10 Mbar by W. J. Nellis, J. A. Moriarity, A. C. Mitchell, M. Ross, R. G. Dandrea, N. W. Ashcroft, N. C. Holmes, and G. R. Gathers, Phys. Rev. Lett. **60**, 1414 (1988).
[6] P. Hohenberg and W. Kohn, Phys. Rev. **136**, B864 (1964); W. Kohn and L. J. Sham, Phys. Rev. **140**, A1133 (1965).
[7] L. Hedin and B. I. Lundqvist, J. Phys. C **4**, 2064 (1971).
[8] J. P. Perdew, in *Electronic Structure of Solids*, edited by P. Ziesche and H. Eschrig (Academic Verlag, Berlin, 1991), p. 11; J. P. Perdew, J. A. Chevary, S. H. Vosko, K. A. Jackson, M. R. Pederson, D. J. Singh, and C. Fiolhais, Phys. Rev. B **46**, 6671 (1992).
[9] B. K. Godwal and R. Jeanloz, Phys. Rev. B **40**, 7501 (1989).
[10] A. Khein, D. J. Singh, and C. J. Umrigar, Phys. Rev. B **51**, 4105 (1995).
[11] T. Korhonen, M. J. Puska, and R. M. Nieminen, Phys. Rev. B **51**, 9526 (1995).
[12] M. J. Mehl and D. A. Papaconstantopoulos, Phys. Rev. B **54**, 4519 (1996).
[13] S. Suzuki and K. Nakao, J. Phys. Soc. Jpn. **68**, 1982 (1999).
[14] P. H. T. Philipsen and E. J. Baerends, Phys. Rev. B **61**, 1773 (2000).
[15] R. Ahuja, S. Rekhi, and B. Johansson, Phys. Rev. B **63**, 212101 (2001).
[16] T. Tsuchiya and K. Kawamura, J. Chem. Phys. **116**, 2121 (2002).
[17] H. L. Skriver, Phys. Rev. B **31**, 1909 (1985).
[18] J. M. Wills, O. Eriksson, P. Söderlind, and A. M. Boring, Phys. Rev. Lett. **68**, 2802 (1992).
[19] G. W. Fernando, R. E. Watson, M. Weinert, Y. J. Wang, and J. W. Davenport, Phys. Rev. B **41**, 11 813 (1990).
[20] J. C. Boettger, Phys. Rev. B **57**, 8743 (1998).
[21] M. D. Jones, J. C. Boettger, R. C. Albers, and D. J. Singh, Phys. Rev. B **61**, 4644 (2000).
[22] J. C. Boettger, Phys. Rev. B **62**, 7809 (2000).
[23] J. C. Boettger, Int. J. Quantum Chem., Symp. **27**, 147 (1993); J. C. Boettger and S. B. Trickey, Phys. Rev. B **32**, 1356 (1985); J. W. Mintmire, J. R. Sabin, and S. B. Trickey, Phys. Rev. B **26**, 1743 (1982).
[24] U. Birkenheuer, J. C. Boettger, and N. Rösch, J. Chem. Phys. **100**, 6826 (1994); U. Birkenheuer, Ph.D. thesis, TU München, 1994.
[25] J. C. Boettger, Int. J. Quantum Chem., Symp. **29**, 197 (1995).
[26] M. Douglas and N. M. Kroll, Ann. Phys. (N.Y.) **82**, 89 (1974).
[27] B. A. Hess, Phys. Rev. A **33**, 3742 (1986); G. Jansen and B. A. Hess, *ibid.* **39**, 6016 (1989); N. J. M. Geipel and B. A. Hess, Chem. Phys. Lett. **273**, 62 (1997).
[28] N. Rösch and O. D. Häberlen, J. Chem. Phys. **96**, 6322 (1992); O. D. Häberlen, and N. Rösch, Chem. Phys. Lett. **199**, 491 (1992); O. D. Häberlen, Ph.D. thesis, Technische Universität München, 1993.
[29] O. Gropen, J. Comput. Chem. **8**, 982 (1987).
[30] The spin-polarized LDA atom energies found here were −37947.26670 Ry without SOC and −37996.55561 Ry with SOC. The equivalent GGA values were −37975.17600 Ry without SOC and −38024.48883 Ry with SOC.
[31] A. B. Alchagirov, J. P. Perdew, J. C. Boettger, R. C. Albers, and C. Fiolhais, Phys. Rev. B **63**, 224115 (2001).
[32] K. A. Gschneidner, Jr., Solid State Phys. **16**, 275 (1964).
[33] Y. M. Juan and E. Kaxiras, Phys. Rev. B **48**, 14 944 (1989).
[34] W. B. Holzapfel, M. Hartwig, and W. Sievers, J. Phys. Chem. Ref. Data **30**, 515 (2001).
[35] J. B. Neaton and N. W. Ashcroft, Nature (London) **400**, 141 (1999).
[36] M. I. McMahon, S. Rekhi, and R. J. Nelmes, Phys. Rev. Lett. **87**, 055501 (2001); R. J. Nelmes, M. I. McMahon, J. S. Loveday, and S. Rekhi, *ibid.* **88**, 155503 (2002).
[37] J. C. Boettger and S. B. Trickey, Phys. Rev. B **32**, 3391 (1985).
[38] A. K. McMahan, Phys. Rev. B **29**, 5982 (1984).